JOURNAL OF AGRICULTURAL AND FOOD CHEMISTRY

pubs.acs.org/JAFC Article

Glutamate Oxidase-Integrated Biomimetic Metal−Organic Framework Hybrids as Cascade Nanozymes for Ultrasensitive Glutamate Detection

Hongtong Hu, Peikun Li, Zichen Wang, Yingjie Du,* Geling Kuang, Yuxiao Feng, Shiru Jia, and Jiandong Cui*

Cite This: *J. Agric. Food Chem.* 2022, 70, 3785−3794 Read Online

ACCESS | Metrics & More | Article Recommendations | Supporting Information

ABSTRACT: The hybrid coupling of biocatalysts and chemical catalysts plays a vital role in the fields of catalysis, sensing, and medical treatment due to the integrated advantages in the high activity of natural enzymes and the excellent stability of nanozymes. Herein, a new nanozyme/natural enzyme hybrid biosensor was established for ultrasensitive glutamate detection. The MIL-88B(Fe)-NH_2 material with remarkable peroxidase mimic activity and stability was used as a nanozyme and carrier for immobilizing glutamate oxidase (GLOX) through Schiff base reaction to construct a chem-enzyme cascade detector (MIL-88B(Fe)-NH_2@GLOX). The resultant MIL-88B(Fe)-NH_2@GLOX exhibited a wide linear range (1−100 μM), with a low detection limit of 2.5 μM for glutamate detection. Furthermore, the MIL-88B(Fe)-NH_2@GLOX displayed excellent reusability and storage stability. After repeated seven cycles, MIL-88B(Fe)-NH_2-GLOX (GLOX was adsorbed on MIL-88B(Fe)-NH_2) lost most of its activity, whereas MIL-88B(Fe)-NH_2@GLOX still retained 69% of its initial activity. Meanwhile, MIL-88B(Fe)-NH_2@GLOX maintained 60% of its initial activity after storage for 90 days, while free GLOX only retained 30% of its initial activity. This strategy of integrating MOF mimics and natural enzymes for cascade catalysis makes it possible to design an efficient and stable chemo-enzyme composite catalysts, which are promising for applications in biosensing and biomimetic catalysis.

KEYWORDS: *metal−organic framework, biomimetic catalysis, chemo-enzymes, biosensing, glutamate detection*

INTRODUCTION

Glutamate, as a flavoring agent and nutrient, widely exists in a variety of foods such as meat, eggs, milk, and vegetables,[1−3] which plays a vital role in the physiological and pathological process of the brain.[4−6] In addition, glutamate is a biomarker of diseases such as cardiomyocytes, hepatocytes, and cancer cells.[7−9] Under normal physiological conditions, the level of glutamate in blood and brain tissue cell fluid is in the range of 150−350 and 50−350 μM, respectively.[5] Therefore, the accurate detection of glutamate concentration is very necessary. Up to now, methods for detecting glutamate mainly include chromatographic, spectrophotometric, capillary electrophoresis techniques, optical, potentiometric, chromatographic techniques, liquid chromatographic, titration, and fluorimeters.[10−14] However, these methods are usually expensive, time-consuming, poor selectivity, and complex to operate. In comparison, colorimetric biosensing methods have the advantages of fast response, simple operation, and high sensitivity, which have been widely used.[15−17] In recent years, biosensors based on inorganic nanomaterials have attracted a lot of attention due to their superior stability, easy preparation, controllable structure, and tunable catalytic sites.[18,19] Especially, biomimetic nanomaterials have been developed rapidly for biosensor detection with the discovery of nanozymes.[20−25] Among them, biomimetic metal−organic frameworks (MOFs) exhibit superior performances.[26−28]

MOFs, as a kind of porous coordination polymers, which were constructed by self-assembly of organic ligands and metal ions or metal clusters, have been used in the fields of gas separation,[29,30] storage and conversion,[31−34] and drug delivery and catalysis[35−38] due to their large specific surface area, permanent pores, adjustable topology, and superior structural stability.[39−41] Furthermore, MOFs have emerged as excellent carriers for immobilized enzymes.[42−44] Recently, some MOFs have been proved with excellent peroxidase-like activity, which promotes their combination with natural enzymes for applications in biosensor detection.[45−48] By coupling the MOFs with peroxidase-like with natural enzymes, a nanozyme/natural enzyme hybrid could be established, which could greatly short the reaction time and show the protective effect of the MOFs on the enzyme.[49,50] Furthermore, the combination of chemo- and enzyme catalysis not only reduces the mass transfer resistance of the reaction but also improves the stability of the enzyme and the sensitivity of detection.[51,52]

Herein, MIL-88B(Fe)-NH_2 (a kind of MOF material, which is composed of Fe^{3+} and 2-aminoterephthalic acid, named as

Received: March 7, 2022
Revised: March 10, 2022
Accepted: March 11, 2022
Published: March 18, 2022

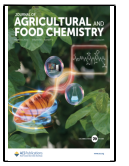

https://doi.org/10.1021/acs.jafc.2c01639
J. Agric. Food Chem. 2022, 70, 3785−3794

Scheme 1. (a) Schematic for the Synthesis Process of MIL-88B(Fe)-NH_2@GLOX and (b) Cascade Catalytic Reaction of MIL-88B(Fe)-NH_2@GLOX for Glutamate Colorimetric Detection

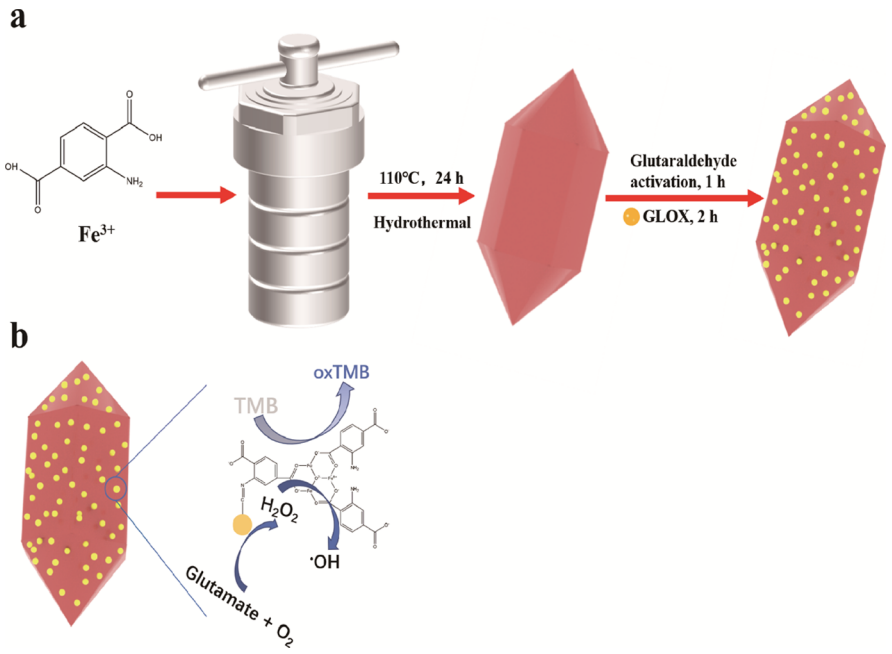

Materials of Institute Lavoisior-88(Fe)-NH_2) with excellent peroxidase-like activity was used as a carrier to integrate GLOX for constructing chemo-enzyme biosensors for glutamate colorimetric detection (Scheme 1a). The working principle of this work is as follows: first, GLOX catalytic oxidation of 1 μmol glutamate to produce 1 μmol H_2O_2, and then, the MIL-88B(Fe)-NH_2 nanoenzyme with peroxidase activity further oxidizes H_2O_2 to generate $^{\bullet}OH$, which can oxidize colorless TMB into blue ox-TMB. It has a strong absorbance value at 652 nm, and a linear relationship can be established between the absorbance value and H_2O_2 (or glutamate) in a certain concentration range. Therefore, the corresponding glutamate concentration can be calculated. Owing to the nanoscale proximity effects, H_2O_2 generated from the GLOX-catalyzed oxidation of glutamate with O_2 will immediately be in situ oxidized by Fe-MOF, diminishing the effect of diffusion resistance and minimization of the decomposition of H_2O_2 (Scheme 1b). The chemo-enzyme catalyst [MIL-88B(Fe)-NH_2@GLOX] not only realizes the rapid and highly sensitive detection of glutamate but also improves the stability and reusability of GLOX. Notably, the strategy of integrating natural enzymes and chemical catalysts successfully retains their excellent properties, which provides an efficient strategy in colorimetric biosensor detection.

EXPERIMENTAL SECTION

Materials. GLOX was extracted and purified from recombinant *Escherichia coli* BL21 (DE3) strain preserved in our laboratory. Pluronic F127 was purchased from Sigma-Aldrich. 3,3′,5,5′-Tetramethylbenzidine (TMB), 2-aminoterephthalic acid (NH_2-BDC), iron(III) chloride hexahydrate ($FeCl_3{\cdot}6H_2O$), horseradish peroxidase (HRP), and glutaraldehyde were purchased from Aladdin (Shanghai, China). Acetic acid, H_2O_2, and FITC were purchased from Shanghai McLean Biochemical Technology Co., Ltd. Glutamate was purchased from Beijing Solarbio Technology Co., Ltd. 4-Hydroxyethyl piperazine ethanesulfonic acid (Hepes) was purchased from Shanghai Yuanye Biotechnology Co., Ltd. All reagents were used without further purification.

Characterization. UV−visible spectra were recorded using UV-2550 PC (Shimadzu, Japan). Field-emission high-resolution scanning electron microscopy (SEM) images were obtained by FEI-Apreo (Czech Republic, USA). Transmission electron microscopy (TEM) and energy spectrum measurements were performed on Talos F200X G2 (Thermo Fisher, USA). X-ray diffraction (XRD) patterns were obtained from U1TIMA IV (Rigaku Corporation, Japan). Fourier transform infrared (FTIR) spectra were recorded using IS50 (Nicolet, United States). Thermal gravimetric analysis (TGA) measurements were Q50 (TA Instruments Waters LLC, United States). Laser confocal fluorescence images were recorded by FV1000 (Olympus, Japan). Pore sizes were analyzed by the Surface Area and Microporous Analyzer ASAP 2020 (micromeritics, USA). Zeta Potentials were measured by the zeta potential analyzer NanoPlus (micromeritics, USA).

Synthesis of MIL-88B(Fe)-NH_2. The synthesis of MIL-88B(Fe)-NH_2 was performed according to the previous report.[53] Typically, 0.64 g of F127 was dissolved in 53.36 mL of deionized water and mixed with 6.64 mL of 0.4 M aqueous solution of $FeCl_3{\cdot}6H_2O$. After stirring for 1 h, 0.9 mL of acetic acid was added. Subsequently, 240 mg (1.32 mmol) of H_2N-BDC was added to the abovementioned solution. After stirring for 2 h, the mixed solution was transferred to an autoclave for reaction at 110 °C for 24 h. After natural cooling, it was centrifuged and washed with absolute ethanol for three times and then dried at 60 °C vacuum overnight to obtain a dark brown solid.

Preparation of MIL-88B(Fe)-NH_2@GLOX and MIL-88B(Fe)-NH_2-GLOX. For preparation of MIL-88B(Fe)-NH_2@GLOX, 10 mg of MIL-88B(Fe)-NH_2 was added to 10 mL of deionized water and treated by ultrasound for 30 min. Then, 0.2 mL of glutaraldehyde solution (50%) was added into the abovementioned solution and stirred for 1 h. After the reaction, the precipitate was recovered by centrifugation, washed twice with deionized water, and resuspended in 7.5 mL of Hepes buffer (20 mM, pH 7.0). Subsequently, 2.5 mL of GLOX solution (11.3 U/mL) was added to the abovementioned Hepes buffer solution. After stirring for 1 h, the precipitate was recovered by centrifugation, washed twice with Hepes buffer solution, and resuspended in 10 mL of Hepes buffer solution for further use. As a comparison, MIL-88B(Fe)-NH_2-GLOX [GLOX was adsorbed on the surface of MIL-88B(Fe)-NH_2] was also prepared; apart from not adding glutaraldehyde solution, other preparation conditions were

https://doi.org/10.1021/acs.jafc.2c01639
J. Agric. Food Chem. 2022, 70, 3785−3794

consistent with those of MIL-88B(Fe)-NH_2@GLOX. See ref 53 for the detection method of enzyme activity.

Synthesis of FITC-Labeled GLOX. 2.5 mg of FITC was dissolved in 1 mL of DMSO and mixed with 5 mL of carbonate buffer (10 mM, pH 9.8) containing GLOX. After stirring for 3 h, the residual FITC was then removed by dialysis with carbonate buffer (10 mM, pH 9.8), and finally, the labeled enzyme solution was immobilized and observed by CLSM.

Peroxidase-Like Activity of MIL-88B(Fe)-NH_2. The peroxidase-like activity of MIL-88B(Fe)-NH_2 was detected using TMB and H_2O_2 as substrates. First, 850 μL of HAc-NaAc buffer solution (0.2 M, pH 4.0) was mixed with 50 μL of TMB ethanol solution (25 mM) and 50 μL of H_2O_2 solution (2 mM). Subsequently, 50 μL of MIL-88B(Fe)-NH_2 solution (1 mg/mL) was added. After reacting at 37 °C for 5 min, the reaction solution was filtered by a 0.22 μM water filtration membrane, and the absorbance value of the resultant filtrate at 652 nm was measured by a UV−vis spectrophotometer. The relative activity was expressed as the ratio of each enzyme activity value to the maximum value of total enzyme activity, and the maximum value of total enzyme activity was defined as 100%. In addition, the optimum reaction pH and temperature of MIL-88B(Fe)-NH_2 were also tested.

Colorimetric Detection of Glutamate. For the colorimetric reaction of glutamate, 100 μL of MIL-88B(Fe)-NH_2@GLOX (1 mg/mL) was mixed with 350 μL of HAc-NaAc buffer (0.2 M, pH 4.0), 50 μL of TMB (25 mM), and 500 μL of glutamate solution with different concentrations. The mixture solution was incubated at 37 °C for 20 min. MIL-88B(Fe)-NH_2@GLOX nanoparticles in the mixture were removed by using a 0.22 μm PTEE microporous filtration membrane, and the absorbance value of the supernatant at 652 nm was measured by using a UV−vis spectrophotometer. As a comparison, MIL-88B(Fe)-NH_2-GLOX was also used to detect colorimetric reaction of glutamate.

Real Sample Detection. Randomly selected three kinds of common processed foods: salad juice, strawberry jam, and milk powder and they were purchased from a local store. An appropriate dissolution method with some modification was adopted according to ref 54 for each sample to gain soluble L-glutamate. 0.5 g of salad juice and strawberry jam was dissolved in 5 mL of Hepes solution (20 mM, pH 7), then ultrasonicated for 10 min, and centrifuged at 8000 rpm for 10 min to gain the supernatant. After filtering by 0.22 μm filter membrane, dilute supernatant by a certain multiple for detection according to colorimetric detection of glutamate. Then, according to the standard detection curve obtained by the biosensor, the concentration of glutamate in the corresponding product was calculated. As for milk powder, taking 0.5g and dissolved it with 5ml boiling Hepes solution and incubated for 10 min. The subsequent steps were the same as that of salad juice.

Effects of pH and Temperature on Cascade Enzymatic Activity of MIL-88B(Fe)-NH_2@GLOX. The effect of pH on the cascade enzymatic activity of MIL-88B(Fe)-NH_2@GLOX was investigated at 37 °C under different pH values: 3.0−10.0. The effect of temperature on cascade enzymatic activity of MIL-88B(Fe)-NH_2@GLOX was determined after incubation in HAc-NaAc buffer (350 μL, 0.2 M, pH 4.0) in the range of 35−70 °C. The rest of the procedures were the same as the colorimetric detection of glutamate.

pH Stability. MIL-88B(Fe)-NH_2@GLOX and MIL-88B(Fe)-NH_2-GLOX were added to different pH values (3−10) buffer solution and incubated for 1 h at room temperature. Subsequently, cascade catalytic activity of MIL-88B(Fe)-NH_2@GLOX and MIL-88B(Fe)-NH_2-GLOX was determined based on the colorimetric detection of glutamate.

Thermal Stability. MIL-88B(Fe)-NH_2@GLOX and MIL-88B-(Fe)-NH_2-GLOX were added in pH 7 Hepes buffer solution (pH 7, 20 mM) and incubated for different times (0, 20, 40, 60, 80, and 100 min) at 50 °C, respectively. Cascade catalytic activity was detected based on the colorimetric detection of glutamate.

Denaturant Stability. MIL-88B(Fe)-NH_2@GLOX and MIL-88B(Fe)-NH_2-GLOX were added in different denaturant solutions (50% ethanol solution, 6 M urea solution, 50% THF solution, and 50% DMSO solution) and incubated for 1 h at room temperature, respectively. Cascade catalytic activity was detected based on the colorimetric detection of glutamate.

Reusability and Storage Stability. The reusability of MIL-88B(Fe)-NH_2@GLOX and MIL-88B(Fe)-NH_2-GLOX was tested by repetitive measurements of cascade catalytic activity. After each reaction, the MIL-88B(Fe)-NH_2@GLOX or MIL-88B(Fe)-NH_2-GLOX was recovered, washed with Hepes buffer solution (pH 7, 20 mM), and then added to the next cycle. The storage stability of free GLOX and MIL-88B(Fe)-NH_2@GLOX was investigated at 25 °C for 90 days, and their cascade catalytic activities were assayed every 10 days.

RESULTS AND DISCUSSION

Characterization of MIL-88B(Fe)-NH_2@GLOX. SEM images of MIL-88B(Fe)-NH_2 and MIL-88B(Fe)-NH_2@GLOX are shown in Figure 1. It can be clearly seen that

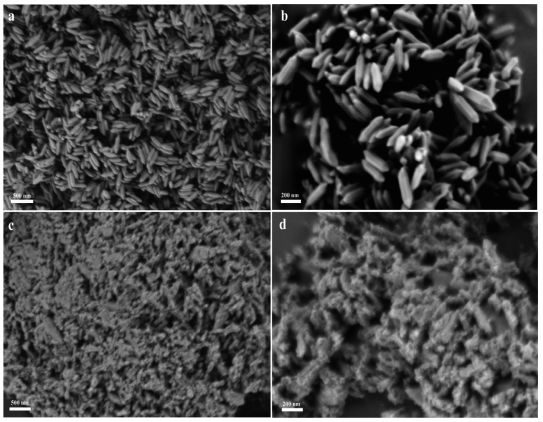

Figure 1. SEM images of (a,b) MIL-88B(Fe)-NH_2 and (c,d) MIL-88B(Fe)-NH_2@GLOX.

MIL-88B(Fe)-NH_2 exhibits a uniform spindle-shaped structure, which is consistent with the previous work.[55] After GLOX molecules were immobilized on the surface of MIL-88B(Fe)-NH_2 with abundant amino groups via aldehyde amine condensation induced by glutaraldehyde, morphology of MIL-88B(Fe)-NH_2@GLOX did not change, and only the surface of MIL-88B(Fe)-NH_2@GLOX was not as smooth as MIL-88B(Fe)-NH_2. GLOX was from *Streptomyces* sp. X-119-6[56] with the molecule size of 12.4 × 12.4 × 16.9 nm. Thus, after immobilization of GLOX on MIL-88B(Fe)-NH_2, the morphology of the MIL-88B(Fe)-NH_2@GLOX particle turns rougher than that of the MIL-88B(Fe)-NH_2 particle, which is consistent with previous reports.[52] The uniform spindle-shaped structure of MIL-88B(Fe)-NH_2@GLOX was further confirmed by TEM (Figure 2a,b). It was indicated that the presence of GLOX had no influence on the morphology of the MIL-88B(Fe)-NH_2.

EDS mapping of elemental distributions of MIL-88B(Fe)-NH_2 and MIL-88B(Fe)-NH_2@GLOX is shown in Figures S1 and 2c, respectively. The C, N, O, and Fe elements can be observed in both MIL-88B(Fe)-NH_2 and MIL-88B(Fe)-NH_2@GLOX, which prove the formation of MIL-88B(Fe)-NH_2. However, only S and P elements were observed in MIL-88B(Fe)-NH_2@GLOX, indicating that GLOX was successfully immobilized on MIL-88B(Fe)-NH_2.

Besides, XRD was used to characterize the crystal structures of MIL-88B(Fe)-NH_2 and MIL-88B(Fe)-NH_2@GLOX. As shown in Figure 3a, the XRD pattern of MIL-88B(Fe)-NH_2 was consistent with MIL-88B(Fe)-NH_2@GLOX, further

https://doi.org/10.1021/acs.jafc.2c01639
J. Agric. Food Chem. 2022, 70, 3785−3794

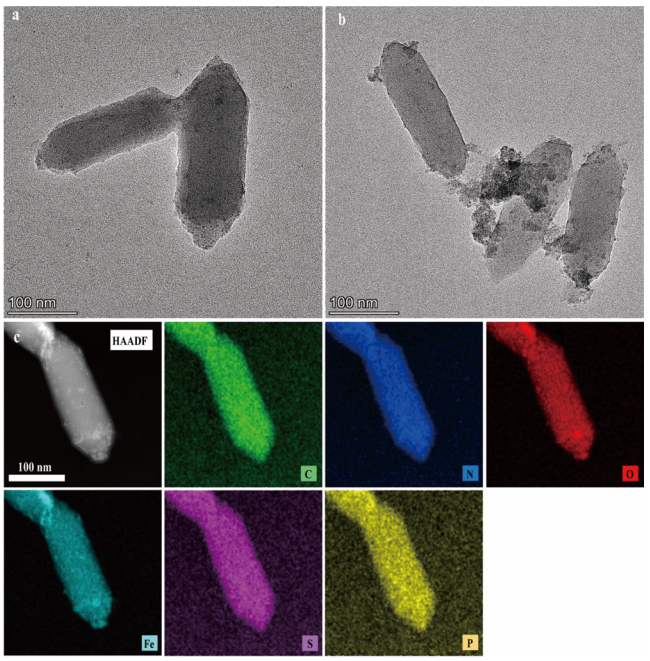

Figure 2. TEM images of (a) MIL-88B(Fe)-NH_2 and (b) MIL-88B(Fe)-NH_2@GLOX. EDS mapping of elemental distributions of (c) MIL-88B(Fe)-NH_2@GLOX for C, N, O, Fe, S, and P.

confirming that the immobilization of GLOX does not destroy the crystal morphology of MIL-88B(Fe)-NH_2.

To further prove that GLOX was successfully immobilized on MIL-88B(Fe)-NH_2, GLOX was first labeled with fluorescein FITC and immobilized on MIL-88B(Fe)-NH_2. The resultant MIL-88B(Fe)-NH_2@GLOX was tested by CLSM. As shown in Figure S2, the green fluorescence could be clearly observed in the CLSM images of the MIL-88B(Fe)-NH_2@GLOX, indicating that GLOX was successfully immobilized to MIL-88B(Fe)-NH_2. Furthermore, as shown in Figure 3b, characteristic peaks at 1707 cm^{-1} with slight shifting compared with the free enzyme (1640 cm^{-1}) in MIL-88B(Fe)-NH_2@GLOX were ascribed to the stretching vibration of the protein-specific amide I bonds (C═O).[57] However, the stretching vibration peak of the amide I bond (C═O) was not observed in MIL-88B(Fe)-NH_2. Moreover, characteristic peaks at 1203^{-} and 1281 cm^{-1} were existed in MIL-88B(Fe)-NH_2@GLOX, indicating the existence of Schiff base.[58] The abovementioned results indicated the existence of GLOX in MIL-88B(Fe)-NH_2@GLOX. TGA results showed that the main weight loss of MIL-88B(Fe)-NH_2@GLOX occurred from 220 to 550 °C can be due to thermal degradation of the enzyme protein molecules and carriers. It is obvious that in the range of 220−330 °C, the mass of MIL-88B(Fe)-NH_2@GLOX is significantly reduced, while the mass of MIL-88B(Fe)-NH_2 is almost unchanged, further proving the presence of GLOX on MIL-88B(Fe)-NH_2 (Figure 3c). Zeta potential measurement (Figure 3d) of MIL-88B(Fe)-NH_2 and MIL-88B(Fe)-NH_2@

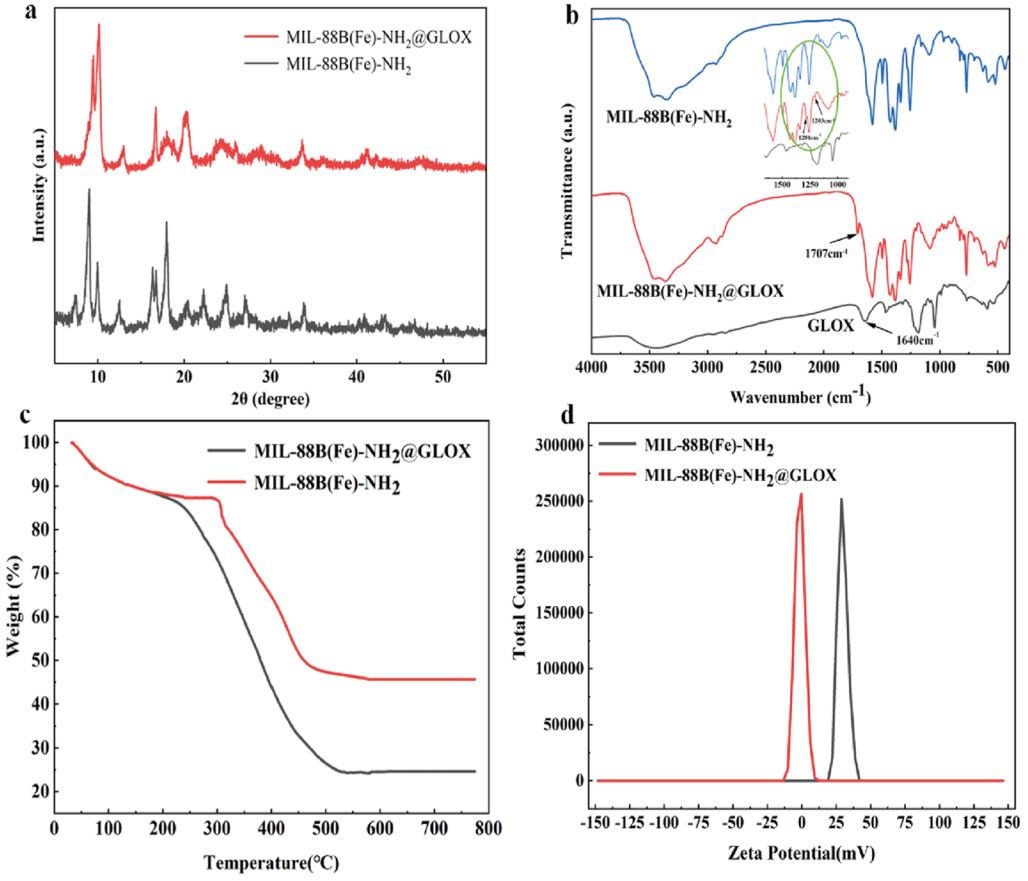

Figure 3. (a) XRD patterns of MIL-88B(Fe)-NH_2 and MIL-88B(Fe)-NH_2@GLOX. (b) FTIR spectra of MIL-88B(Fe)-NH_2, GLOX, and MIL-88B(Fe)-NH_2@GLOX. (c) TGA curves of MIL-88B(Fe)-NH_2 and MIL-88B(Fe)-NH_2@GLOX. (d) Zeta Potential of MIL-88B(Fe)-NH_2 and MIL-88B(Fe)-NH_2@GLOX.

https://doi.org/10.1021/acs.jafc.2c01639
J. Agric. Food Chem. 2022, 70, 3785−3794

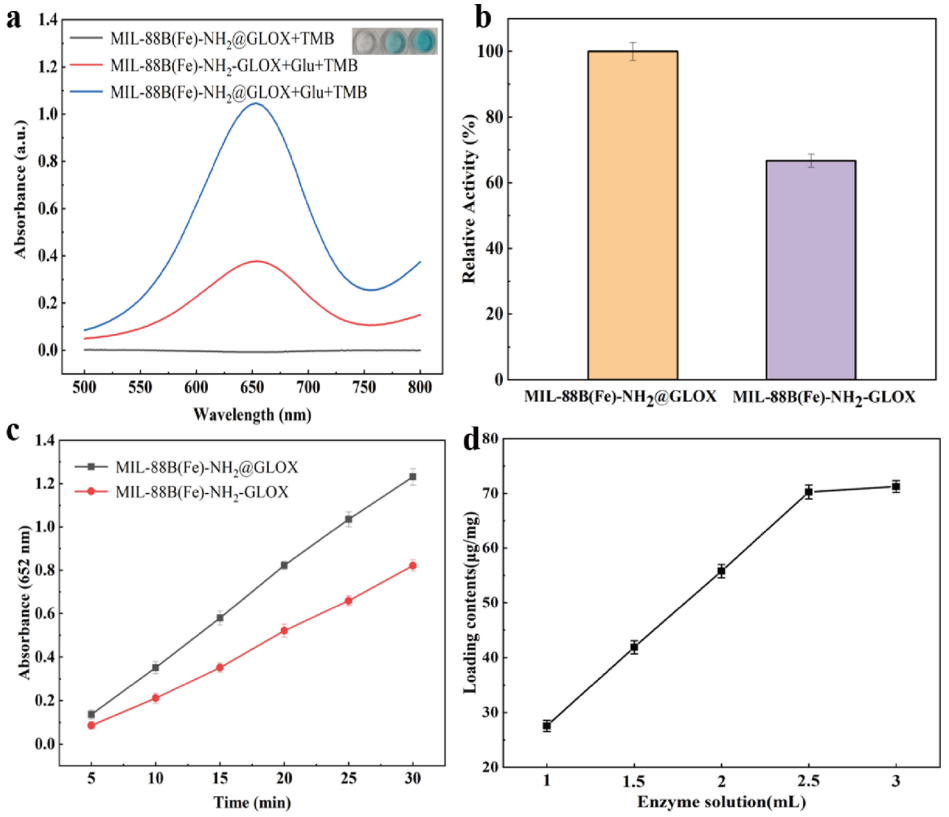

Figure 4. (a) UV−vis spectra and digital photograph (inset) of cascade reaction of the MIL-88B(Fe)-NH_2-GLOX and MIL-88B(Fe)-NH_2@GLOX (2.5 mM TMB and 200 μM glutamate were incubated in 0.2 M pH 4.0 Hac-NaAc buffer solution at 37 °C for 20 min). (b) Relative activity of cascade reaction for MIL-88B(Fe)-NH_2@GLOX and MIL-88B(Fe)-NH_2-GLOX. (c) Time−absorbance curve of MIL-88B(Fe)-NH_2@GLOX and MIL-88B(Fe)-NH_2-GLOX in 200 μM glutamate. (d) Loading contents of GLOX on MIL-88B(Fe)-NH_2 (1, 1.5, 2, 2.5, and 3 mL of enzyme solution (140 μg/mL) were added to MIL-88B(Fe)-NH_2 solution (1 mg/mL, total volume was 5 mL). After the reaction is complete, the protein concentration (BCA method) was detected in the supernatant to calculate loading contents of GLOX on MIL-88B(Fe)-NH_2). The data were shown as mean ± SD (n = 3).

GLOX indicates that after GLOX being immobilized on MIL-88B(Fe)-NH_2, the apparent potential of MIL-88B(Fe)-NH_2@GLOX was changed from the positive potential of MIL-88B(Fe)-NH_2 to negative potential. The pore size analysis result in Figure S8 shows that the immobilization of GLOX on MIL-88B(Fe)-NH_2 cannot obviously affect the pore size.

Peroxidase-Like Activity of MIL-88B(Fe)-NH_2. Here, the peroxidase-like activity of MIL-88B(Fe)-NH_2 was tested by performing a typical chromogenic reaction. MIL-88B(Fe)-NH_2 catalyzes H_2O_2 to produce $^{\bullet}OH$ (Figure S7), which would further oxidize TMB into the oxidation state of TMB (ox-TMB). Meanwhile, an obvious characteristic absorption peak at 652 nm could be observed. However, no absorption peak at 652 nm was observed for individual TMB and TMB/H_2O_2, suggesting the high peroxidase-like activity of MIL-88B(Fe)-NH_2 (Figure S3). Besides, effects of pH and temperature on peroxidase-like activity of MIL-88B(Fe)-NH_2 were also studied. As shown in Figure S4, the optimum pH of MIL-88B(Fe)-NH_2 is pH 4.0. Meanwhile, within a certain range, the absorbance increases with the increase of temperature. Moreover, Michaelis−Menten curves (Figure S5) were tested to confirm the peroxidase-like activity of MIL-88B(Fe)-NH_2. Kinetic parameters of MIL-88B(Fe)-NH_2 including Michaelis constant (K_m) and maximum reaction velocity (V_{max}) are shown in Table S1. MIL-88B(Fe)-NH_2 exhibits smaller K_m (K_m is 0.23 and 2.39 mM using H_2O_2 and TMB as the substrate, respectively) than other peroxidase-like materials (e.g., MOF-808,[49] K_m is 1.06 mM using H_2O_2 as the substrate; Zn-CuO,[59] K_m is 10 mM using TMB as the substrate), indicating the excellent peroxidase-like activity.

Performance of MIL-88B(Fe)-NH_2-GLOX and MIL-88B(Fe)-NH_2@GLOX. Theoretically, GLOX can catalyze glutamate to produce α-ketoglutarate and H_2O_2. Then, H_2O_2 was catalyzed by MIL-88B(Fe)-NH_2 to yield $^{\bullet}OH$, which would further oxidize TMB into the oxidation state of TMB. Subsequently, the linear relationship between the oxidation state of TMB and L-glutamate concentration was established. Therefore, the cascade catalytic performances of MIL-88B-(Fe)-NH_2-GLOX and MIL-88B(Fe)-NH_2@GLOX were compared. As shown in Figure 4a, there are no obvious color change and absorbance value at 652 nm for the MIL-88B(Fe)-NH_2@GLOX/TMB reaction system, indicating that MIL-88B(Fe)-NH_2@GLOX cannot catalyze this cascade reaction in the absence of glutamate. However, when adding glutamate into the MIL-88B(Fe)-NH_2-GLOX/TMB or MIL-88B(Fe)-NH_2@GLOX/TMB reaction system, typical blue-green color could be clearly observed. Furthermore, it was found that the color intensity of MIL-88B(Fe)-NH_2@GLOX/TMB was obviously deeper than that of MIL-88B(Fe)-NH_2-GLOX/TMB. The relative activity (absorbance value at 652 nm) of MIL-88B(Fe)-NH_2@GLOX/TMB was 1.4 times than that of MIL-88B(Fe)-NH_2-GLOX/TMB (Figure 4b). The enhanced catalytic efficiency of MIL-88B(Fe)-NH_2@GLOX/TMB may be due to the following reasons: (1) the close integration of

https://doi.org/10.1021/acs.jafc.2c01639
J. Agric. Food Chem. 2022, 70, 3785−3794

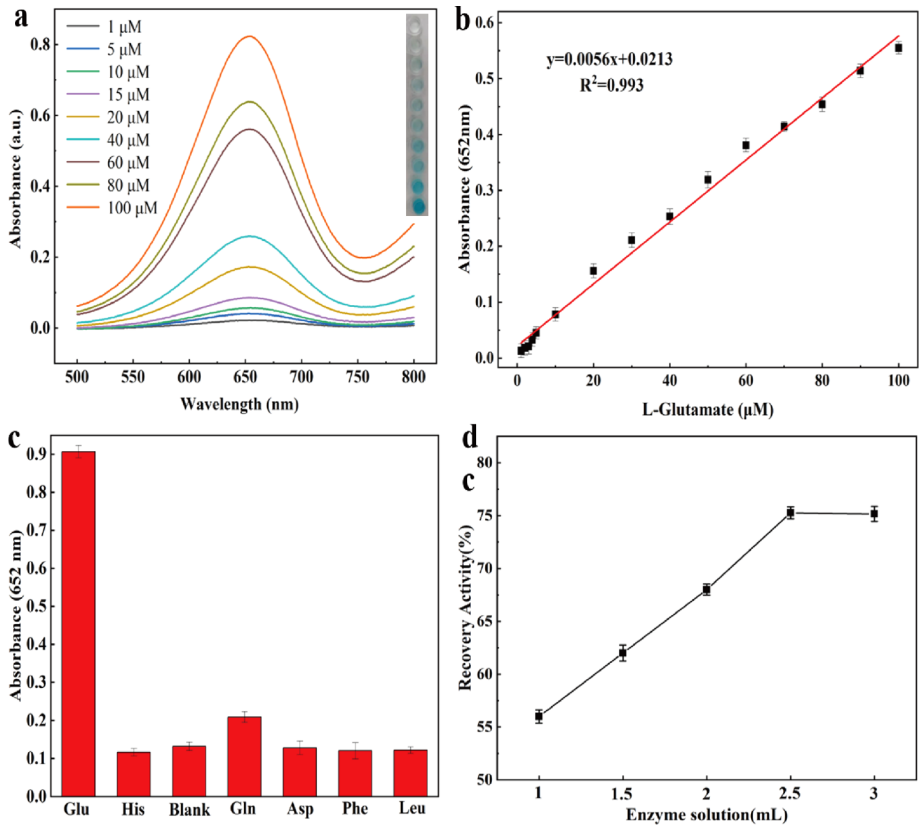

Figure 5. (a) UV−vis spectra and digital photograph (inset) of cascade reaction with the glutamate concentration from 1 to 100 μM and (b) linear calibration curve for glutamate detection at 652 nm. (c) Anti-interference of MIL-88B(Fe)-NH_2@GLOX [from left to right: glutamate (0.2 mM), histidine, blank, glutamine, aspartate, phenylalanine, and leucine]. (d) Recovery activity of GLOX after immobilizing on MIL-88B(Fe)-NH_2 (by detecting Figure 4d immobilized enzyme and free enzyme activity to calculate GLOX recovery activity). The data were shown as mean ± SD (n = 3).

MIL-88B(Fe)-NH_2 and GLOX greatly reduces the mass transfer distance between substrates. (2) The in situ generated H_2O_2 was immediately catalyzed by the adjacent MIL-88B(Fe)-NH_2 to solve self-inactivation of GLOX by H_2O_2. Furthermore, the velocity of the MIL-88B(Fe)-NH_2@GLOX/TMB system was significantly faster than that of the MIL-88B(Fe)-NH_2-GLOX/TMB system. Therefore, the strategy of integrating natural enzymes and chemical catalysts could be an efficient strategy in colorimetric biosensor detection.

Furthermore, through the measurement of the enzyme loading contents (Figure 4d) and enzyme activity recovery (Figure 5d) of the carrier, it was found that with the increasing enzyme addition, the enzyme loading contents and enzyme activity recovery increased continuously, and the maximum value was 70.27 μg/mg and 75.25%, respectively. At low loading contents, the low recovery of enzyme activity may be caused by excessive glutaraldehyde on the surface of carriers.

Effect of pH and Temperature on the Catalysis Activity of MIL-88B(Fe)-NH_2@GLOX. The catalysis activity of MIL-88B(Fe)-NH_2-GLOX and MIL-88B(Fe)-NH_2@GLOX was studied at different pH values (pH 3.0−10.0) and temperatures (35−70 °C). As can be seen in Figure S6a, the optimal pH (4.0) of the cascade reaction is consistent with MIL-88B(Fe)-NH_2. However, the optimal temperature of MIL-88B(Fe)-NH_2@GLOX was higher than that of MIL-88B(Fe)-NH_2-GLOX (Figure S6b). The results could be because the formation of the covalent bond between MIL-88B(Fe)-NH_2 and GLOX increases the rigidity of enzyme conformation, thus improving the resistance of enzymes to temperature. In addition, it was found that MIL-88B(Fe)-NH_2@GLOX exhibited higher pH stability and thermal stability than MIL-88B(Fe)-NH_2-GLOX (data not shown), revealing that the integrated MIL-88B(Fe)-NH_2@GLOX possesses excellent ability against harsh conditions.

Glutamate Detection Using MIL-88B(Fe)-NH_2@GLOX. The performance of the MIL-88B(Fe)-NH_2@GLOX for the assay of glutamate was systematically investigated. As shown in Figure 5a, with the increasing glutamate concentration, the light absorption intensity of the reaction supernatant at 652 nm also increased gradually, suggesting that the MIL-88B(Fe)-NH_2@GLOX exhibited feasibility for the detection of glutamate. Meanwhile, the glutamate concentration and the reaction supernatant absorbance showed a strong linear relationship (R^2 = 0.993) in the range of 1−100 μM with a limit of detection (LOD) of 2.5 μM (S/N = 3) (Figure 5b). Compared this biosensor with other biosensors for glutamate detection (Table S2), for example, Nakorn et al.[S2] embedded GLOX into an electrode and Kaivosoja et al.[S3] immobilized GLOX on the surface of the electrode by absorption, the linear range and sensitivity of both are poor, which may be related to the materials of the electrode and the enzyme immobilization methods, while the established biosensor exhibited a lower linear range and high sensitivity. However, the works of Nakorn et al.[S2] and Tseng et al.[S5] show better reproducibility than this work, while the relatively weak reproducibility of this work was due to the loss of the immobilized enzyme during

https://doi.org/10.1021/acs.jafc.2c01639
J. Agric. Food Chem. 2022, 70, 3785−3794

centrifugation. Furthermore, we found that these previously reported electrochemical detection sensors show weak storage stability, probably caused by the inappropriate enzyme immobilization method. While the colorimetric biosensor possessed excellent storage stability, we speculated that covalent immobilization may maintain the structural stability of enzyme molecules. In fact, this was the first time that the chem-enzyme biosensor was used for colorimetric detection of glutamate, which was different from the traditional electrochemical detection sensor and there were differences in related performance between them naturally. In short, this detection method showed considerable advantages.

Besides, the selectivity and anti-interference ability of MIL-88B(Fe)-NH_2@GLOX were assessed by detecting the absorbance values (A652) in the presence of different interferents such as aspartate, histidine, phenylalanine, and leucine. Although the concentrations of aspartate, histidine, phenylalanine, and leucine were 10-fold higher than that of glutamate, no distinct signal interference was observed (Figure 5c), indicating that MIL-88B(Fe)-NH_2@GLOX possesses a specific response to glutamate.

Real Sample Detection. Many foods in life, especially processed foods, contained a certain amount of glutamate. The intake of glutamate needs to be maintained within a certain range in order not to bring side effects. Therefore, it was necessary to accurately detect the content of glutamate in food. To verify the practicability of our biosensor, we randomly selected several common processed foods as the detection objects, the chemo-enzyme biodetector was applied in real samples for L-glutamate detection. After the sample was pretreated, it was tested, and finally, the concentration of glutamate was converted into the mass percentage of the sample. As shown in Table 1, the L-glutamate concentrations in real samples were in good agreement with that given in the nutrient composition table, and the relative standard deviations (RSD) were less than 4%, suggesting that the biosensor possessed potential possibility for commercial detection.

Table 1. L-Glutamate Contents of Real Samples and RSD Obtained by the Biosensor

real sample	real concentration (%)	biosensor detection (%)	RSD % (n = 3)
salad juice	9−13	11.27	2.7
strawberry jam	1.5−1.8	1.75	2.5
milk powder	0.2−0.4	0.33	3.2

Reusability and Stability of the Immobilized Enzyme. The reusability of MIL-88B(Fe)-NH_2@GLOX and MIL-88B(Fe)-NH_2-GLOX was determined, and results are shown in Figure 6a. After seven repetitions, MIL-88B(Fe)-NH_2@GLOX could still maintain 69% of its initial activity, whereas MIL-88B(Fe)-NH_2-GLOX only retained 20% of its initial activity, indicating that MIL-88B(Fe)-NH_2@GLOX has better reusability than MIL-88B(Fe)-NH_2-GLOX. The excellent reusability of MIL-88B(Fe)-NH_2@GLOX could be due to the fact that GLOX molecules are immobilized on MIL-88B(Fe)-NH_2 by covalent binding. Furthermore, free GLOX lost most of its activity after 90 days of storage, whereas MIL-88B(Fe)-NH_2@GLOX still retained 60% of its initial activity (Figure 6b), suggesting that the biosensor possessed good storage stability.

Besides, the stability of MIL-88B(Fe)-NH_2@GLOX against high temperature, extreme pH, and chemical denaturant was investigated. As shown in Figure 7a, MIL-88B(Fe)-NH_2@GLOX retained higher enzyme activity than MIL-88B(Fe)-NH_2-GLOX under strong acidic/alkaline conditions (pH 3.0 or 10.0), indicating that MIL-88B(Fe)-NH_2@GLOX possesses higher stability against extreme pH than MIL-88B(Fe)-NH_2-GLOX. Meanwhile, MIL-88B(Fe)-NH_2@GLOX maintained 40% of its initial activity after being treated for 100 min at 50 °C, while MIL-88B(Fe)-NH_2-GLOX only retained 8% of its initial activity (Figure 7b). Furthermore, as shown in Figure 7c, MIL-88B(Fe)-NH_2@GLOX exhibited higher stability against the chemical denaturant than MIL-88B(Fe)-NH_2-GLOX. For example, MIL-88B(Fe)-NH_2-GLOX only maintained 10% of its initial activity after being treated with 6 M urea for 1 h, whereas MIL-88B(Fe)-NH_2@GLOX still retained 50% of its initial activity (Figure 7c), suggesting high tolerance of MIL-88B(Fe)-NH_2@GLOX to urea. These results showed that the integration of MIL-88B(Fe)-NH_2 and GLOX could protect form the enzyme and improve the stability of the enzyme, which was conducive to practical application.

In summary, a new nanozyme/natural enzyme hybrid biosensor was established for ultrasensitive glutamate detection based on peroxidase-like MIL-88B(Fe)-NH_2 and GLOX,

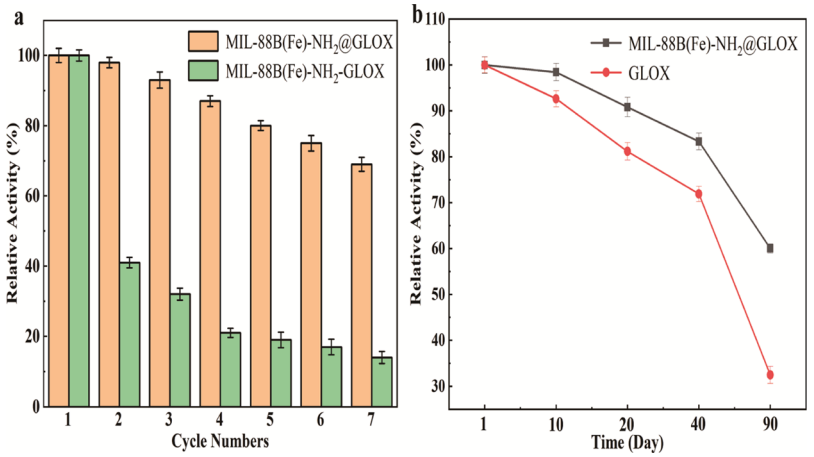

Figure 6. (a) Reusability of MIL-88B(Fe)-NH_2-GLOX and MIL-88B(Fe)-NH_2@GLOX. (b) Storage stability of free GLOX and MIL-88B(Fe)-NH_2@GLOX. The data were shown as mean ± SD (n = 3).

https://doi.org/10.1021/acs.jafc.2c01639
J. Agric. Food Chem. 2022, 70, 3785−3794

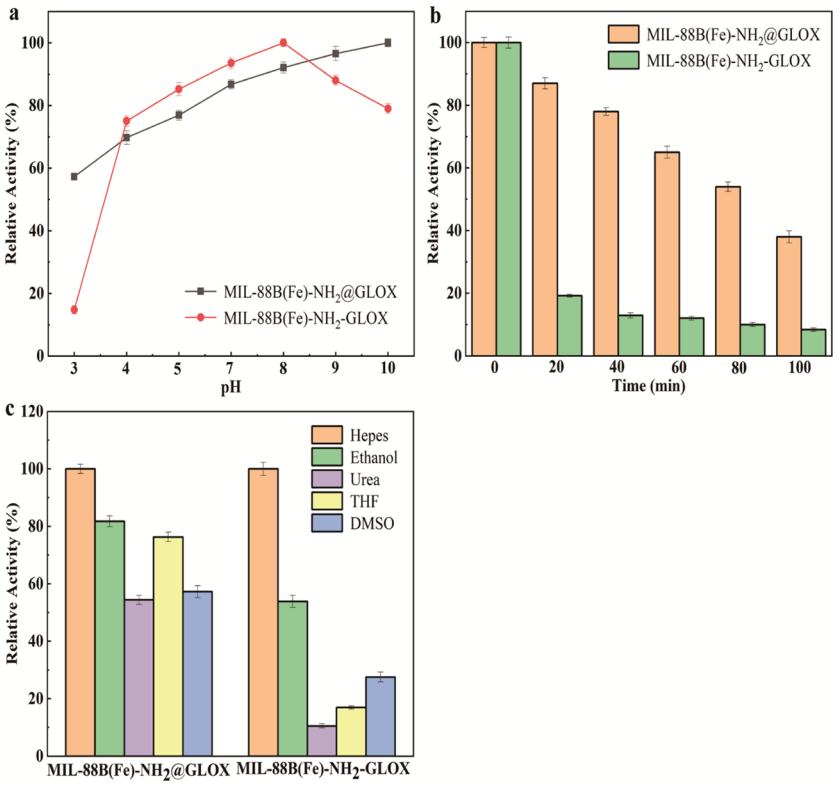

Figure 7. (a) pH stability of MIL-88B(Fe)-NH_2@GLOX and MIL-88B(Fe)-NH_2-GLOX. (b) Thermal stability of MIL-88B(Fe)-NH_2@GLOX and MIL-88B(Fe)-NH_2-GLOX. (c) Stability of MIL-88B(Fe)-NH_2@GLOX and MIL-88B(Fe)-NH_2-GLOX against chemical denaturants. The data were shown as mean ± SD (n = 3).

which integrated the advantages of enhanced activity of the nanozyme and selectivity of the natural enzyme. Compared with the free GLOX, MIL-88B(Fe)-NH_2@GLOX displayed excellent reusability, storage stability and tolerance to high temperature and was an extreme pH and chemical denaturant. Furthermore, the MIL-88B(Fe)-NH_2@GLOX exhibited excellent performances for glutamate detection. Consequently, this strategy of integrating MOF mimics and natural enzymes for cascade catalysis makes it possible to design an efficient and stable chemo-enzyme composite catalyst, which are promising for applications in biosensing and biomimetic catalysis.

■ ASSOCIATED CONTENT

Supporting Information

The Supporting Information is available free of charge at https://pubs.acs.org/doi/10.1021/acs.jafc.2c01639.

EDS mapping, peroxidase-like activity, steady-state kinetic analyses and kinetic parameters of MIL-88B-(Fe)-NH_2; CLSM images of MIL-88B(Fe)-NH_2@GLOX; catalysis activity of MIL-88B(Fe)-NH_2, MIL-88B(Fe)-NH_2@GLOX, and MIL-88B(Fe)-NH_2-GLOX; fluorescence spectra of different reaction systems; pore size distribution of MIL-88B(Fe)-NH_2 and MIL-88B-(Fe)-NH_2@GLOX; comparison of MIL-88B(Fe)-NH_2@GLOX with other biosensors; and comparison of enzyme activity between HRP and MIL-88B(Fe)-NH_2 (PDF)

■ AUTHOR INFORMATION

Corresponding Authors

Yingjie Du − *State Key Laboratory of Food Nutrition and Safety, Laboratory of Industrial Fermentation Microbiology, Ministry of Education, Tianjin University of Science and Technology, Tianjin 300457, P R China;* orcid.org/0000-0002-7291-2098; Phone: +86-022-60602822; Email: yingjiedu@tust.edu.cn

Jiandong Cui − *State Key Laboratory of Food Nutrition and Safety, Laboratory of Industrial Fermentation Microbiology, Ministry of Education, Tianjin University of Science and Technology, Tianjin 300457, P R China;* orcid.org/0000-0002-2809-530X; Email: cjd007cn@163.com

Authors

Hongtong Hu − *State Key Laboratory of Food Nutrition and Safety, Laboratory of Industrial Fermentation Microbiology, Ministry of Education, Tianjin University of Science and Technology, Tianjin 300457, P R China;* orcid.org/0000-0002-8075-7497

Peikun Li − *State Key Laboratory of Food Nutrition and Safety, Laboratory of Industrial Fermentation Microbiology, Ministry of Education, Tianjin University of Science and Technology, Tianjin 300457, P R China*

Zichen Wang − *State Key Laboratory of Food Nutrition and Safety, Laboratory of Industrial Fermentation Microbiology, Ministry of Education, Tianjin University of Science and Technology, Tianjin 300457, P R China*

Geling Kuang − *State Key Laboratory of Food Nutrition and Safety, Laboratory of Industrial Fermentation Microbiology, Ministry of Education, Tianjin University of Science and Technology, Tianjin 300457, P R China*

https://doi.org/10.1021/acs.jafc.2c01639
J. Agric. Food Chem. 2022, 70, 3785−3794

Yuxiao Feng − *State Key Laboratory of Food Nutrition and Safety, Laboratory of Industrial Fermentation Microbiology, Ministry of Education, Tianjin University of Science and Technology, Tianjin 300457, P R China*

Shiru Jia − *State Key Laboratory of Food Nutrition and Safety, Laboratory of Industrial Fermentation Microbiology, Ministry of Education, Tianjin University of Science and Technology, Tianjin 300457, P R China*

Complete contact information is available at: https://pubs.acs.org/10.1021/acs.jafc.2c01639

Notes

The authors declare no competing financial interest.

■ ACKNOWLEDGMENTS

Dr. J. D. Cui thanks supports from the Science and Technology Program of Tianjin, China (project no. 20ZYJDJC00080), the Key Projects of Tianjin Natural Science Foundation, China (project no. 19JCZDJC38100), the National Natural Science Foundation of China (project no. 22108206), Key R & D projects in Zhongning County, China (project no. 2021YBYF0808), project of Key Research and Development of Guangxi province, China (project no. 2021AB20094), project of Key Research and Development of Shandong province, China (project no. 2021CXGC010509), and Postgraduate Research Innovation project of Tianjin (project no. 2020YJSB122).

■ REFERENCES

(1) Ito, H.; Hiroshi, U.; Hiroe, K. Construction of a free-form amino acid database for vegetables and mushrooms. *Integr. Food Nutr. Metab.* **2017**, *4*, 1−9.

(2) Kazmi, Z.; Fatima, I.; Perveen, S.; Malik, S. S. Monosodium glutamate: Review on clinical reports. *Int. J. Food Prop.* **2017**, *20*, 1807−1815.

(3) Krishna Veni, N.; Karthika, D.; Surya Devi, M.; Rubini, M. F.; Vishalini, M.; Pradeepa, Y. J. Analysis of monosodium L-glutamate in food products by high-performance thin layer chromatography. *J. Young Pharm.* **2010**, *2*, 297−300.

(4) Abbott, N. J.; Rönnbäck, L.; Hansson, E. Astrocyte-endothelial interactions at the blood-brain barrier. *Nat. Rev. Neurosci.* **2006**, *7*, 41−53.

(5) Leibowitz, A.; Boyko, M.; Shapira, Y.; Zlotnik, A. Blood glutamate scavenging: Insight into neuroprotection. *Int. J. Mol. Sci.* **2012**, *13*, 10041−10066.

(6) Pardridge, W. M. The blood-brain barrier: Bottleneck in brain drug development. *NeuroRx* **2005**, *2*, 3−14.

(7) Dutta, S.; Ray, S.; Nagarajan, K. Glutamic acid as anticancer agent: An overview. *Saudi Pharm. J.* **2013**, *21*, 337−343.

(8) Shi, Z.; Luscombe-Marsh, N. D.; Wittert, G. A.; Yuan, B.; Dai, Y.; Pan, X.; Taylor, A. W. Monosodium glutamate is not associated with obesity or a greater prevalence of weight gain over 5 years: Findings from the Jiangsu Nutrition Study of Chinese adults. *Br. J. Nutr.* **2010**, *104*, 457−463.

(9) Uchida, Y.; Takio, K.; Titani, K.; Ihara, Y.; Tomonaga, M. The growth inhibitory factor that is deficient in the Alzheimer's disease brain is a 68 amino acid metallothionein-like protein. *Neuron* **1991**, *7*, 337−347.

(10) Cordek, J.; Wang, X.; Tan, W. Direct immobilization of glutamate dehydrogenase on optical fiber probes for ultrasensitive glutamate detection. *Anal. Chem.* **1999**, *71*, 1529−1533.

(11) Eastwood, K.; Else, P.; Charlett, A.; Wilcox, M. Comparison of nine commercially available Clostridium difficile toxin detection assays, a real-time PCR assay for C. difficile tcdB, and a glutamate dehydrogenase detection assay to cytotoxin testing and cytotoxigenic culture methods. *J. Clin. Microbiol.* **2009**, *47*, 3211−3217.

(12) Song, J.; Liang, B.; Han, D.; Tang, X.; Lang, Q.; Feng, R.; Han, L.; Liu, A. Bacterial cell-surface displaying of thermo-tolerant glutamate dehydrogenase and its application in L-glutamate assay. *Enzyme Microb. Technol.* **2015**, *70*, 72−78.

(13) Liang, B.; Zhang, S.; Lang, Q.; Song, J.; Han, L.; Liu, A. Amperometric L-glutamate biosensor based on bacterial cell-surface displayed glutamate dehydrogenase. *Anal. Chim. Acta* **2015**, *884*, 83−89.

(14) Mentana, A.; Nardiello, D.; Palermo, C.; Centonze, D. Accurate glutamate monitoring in foodstuffs by a sensitive and interference-free glutamate oxidase based disposable amperometric biosensor. *Anal. Chim. Acta* **2020**, *1115*, 16−22.

(15) Masud, M. K.; Na, J.; Younus, M.; Hossain, M. S. A.; Bando, Y.; Shiddiky, M. J. A.; Yamauchi, Y. Superparamagnetic nanoarchitectures for disease-specific biomarker detection. *Chem. Soc. Rev.* **2019**, *48*, 5717−5751.

(16) Tanaka, S.; Masud, M. K.; Kaneti, Y. V.; Shiddiky, M. J. A.; Fatehmulla, A.; Aldhafiri, A. M.; Farooq, W. A.; Bando, Y.; Hossain, M. S. A.; Yamauchi, Y. Enhanced peroxidase mimetic activity of porous iron oxide nanoflakes. *Chem. Nano. Mat.* **2019**, *5*, 506−513.

(17) Masud, M. K.; Kim, J.; Billah, M. M.; Wood, K.; Shiddiky, M. J. A.; Nguyen, N.-T.; Parsapur, R. K.; Kaneti, Y. V.; Alshehri, A. A.; Alghamidi, Y. G.; Alzahrani, K. A.; Adharvanachari, M.; Selvam, P.; Hossain, M. S. A.; Yamauchi, Y. Nanoarchitectured peroxidase-mimetic nanozymes: mesoporous nanocrystalline α- or γ-iron oxide? *J. Mater. Chem. B* **2019**, *7*, 5412−5422.

(18) Bhattacharjee, R.; Tanaka, S.; Moriam, S.; Masud, M. K.; Lin, J.; Alshehri, S. M.; Ahamad, T.; Salunkhe, R. R.; Nguyen, N.-T.; Yamauchi, Y.; Hossain, M. S. A.; Shiddiky, M. J. A. Porous nanozymes: the peroxidase-mimetic activity of mesoporous iron oxide for the colorimetric and electrochemical detection of global DNA methylation. *J. Mater. Chem. B* **2018**, *6*, 4783−4791.

(19) Masud, M. K.; Yadav, S.; Islam, M. N.; Nguyen, N.-T.; Salomon, C.; Kline, R.; Alamri, H. R.; Alothman, Z. A.; Yamauchi, Y.; Hossain, M. S. A.; Shiddiky, M. J. A. Gold-loaded nanoporous ferric oxide nanocubes with peroxidase-mimicking activity for electrocatalytic and colorimetric detection of autoantibody. *Anal. Chem.* **2017**, *89*, 11005−11013.

(20) Liang, M.; Yan, X. Nanozymes: From new concepts, mechanisms, and standards to applications. *Acc. Chem. Res.* **2019**, *52*, 2190−2200.

(21) Gao, L.; Zhuang, J.; Nie, L.; Zhang, J.; Zhang, Y.; Gu, N.; Wang, T.; Feng, J.; Yang, D.; Perrett, S.; Yan, X. Intrinsic peroxidase-like activity of ferromagnetic nanoparticles. *Nat. Nanotechnol.* **2007**, *2*, 577−583.

(22) Wei, H.; Wang, E. Fe_3O_4 magnetic nanoparticles as peroxidase mimetics and their applications in H_2O_2 and glucose detection. *Anal. Chem.* **2008**, *80*, 2250−2254.

(23) Cheng, H.; Zhang, L.; He, J.; Guo, W.; Zhou, Z.; Zhang, X.; Nie, S.; Wei, H. Integrated nanozymes with nanoscale proximity for in vivo neurochemical monitoring in living brains. *Anal. Chem.* **2016**, *88*, 5489−5497.

(24) Wu, J.; Wang, X.; Wang, Q.; Lou, Z.; Li, S.; Zhu, Y.; Qin, L.; Wei, H. Nanomaterials with enzyme-like characteristics (nanozymes): next-generation artificial enzymes (II). *Chem. Soc. Rev.* **2019**, *48*, 1004−1076.

(25) Wei, H.; Gao, L.; Fan, K.; Liu, J.; He, J.; Qu, X.; Dong, S.; Wang, E.; Yan, X. Nanozymes: A clear definition with fuzzy edges. *Nano. Today* **2021**, *40*, 101269.

(26) Zhang, M.; Gu, Z.-Y.; Bosch, M.; Perry, Z.; Zhou, H.-C. Biomimicry in metal-organic materials. *Coord. Chem. Rev.* **2015**, *293−294*, 327−356.

(27) Nath, I.; Chakraborty, J.; Verpoort, F. Metal organic frameworks mimicking natural enzymes: a structural and functional analogy. *Chem. Soc. Rev.* **2016**, *45*, 4127−4170.

(28) Chen, K.; Wu, C.-D. Designed fabrication of biomimetic metal-organic frameworks for catalytic applications. *Coord. Chem. Rev.* **2019**, *378*, 445−465.

(29) Zhao, Z.; Ma, X.; Kasik, A.; Li, Z.; Lin, Y. S. Gas separation properties of metal organic framework (MOF-5) membranes. *Ind. Eng. Chem. Res.* **2013**, *52*, 1102−1108.
(30) Luo, F.; Yan, C.; Dang, L.; Krishna, R.; Zhou, W.; Wu, H.; Dong, X.; Han, Y.; Hu, T.-L.; O'Keeffe, M.; Wang, L.; Luo, M.; Lin, R.-B.; Chen, B. UTSA-74: A MOF-74 isomer with two accessible binding sites per metal center for highly selective gas separation. *J. Am. Chem. Soc.* **2016**, *138*, 5678−5684.
(31) Alezi, D.; Belmabkhout, Y.; Suyetin, M.; Bhatt, P. M.; Weseliński, Ł. J.; Solovyeva, V.; Adil, K.; Spanopoulos, I.; Trikalitis, P. N.; Emwas, A.-H.; Eddaoudi, M. MOF crystal chemistry paving the way to gas storage needs: Aluminum-based soc-MOF for CH_4, O_2, and CO_2 storage. *J. Am. Chem. Soc.* **2015**, *137*, 13308−13318.
(32) Chen, Z.; Adil, K.; Weseliński, Ł. J.; Belmabkhout, Y.; Eddaoudi, M. A supermolecular building layer approach for gas separation and storage applications: The eea and rtl MOF platforms for CO_2 capture and hydrocarbon separation. *J. Mater. Chem. A* **2015**, *3*, 6276−6281.
(33) Zou, R.; Li, P.-Z.; Zeng, Y.-F.; Liu, J.; Zhao, R.; Duan, H.; Luo, Z.; Wang, J.-G.; Zou, R.; Zhao, Y. Bimetallic metal-organic frameworks: Probing the Lewis acid site for CO_2 conversion. *Small* **2016**, *12*, 2334−2343.
(34) Han, Y.; Xu, H.; Su, Y.; Xu, Z.-l.; Wang, K.; Wang, W. Noble metal (Pt, Au@Pd) nanoparticles supported on metal organic framework (MOF-74) nanoshuttles as high-selectivity CO_2 conversion catalysts. *J. Catal.* **2019**, *370*, 70−78.
(35) Gandara-Loe, J.; Souza, B. E.; Missyul, A.; Giraldo, G.; Tan, J.-C.; Silvestre-Albero, J. MOF-based polymeric nanocomposite films as potential materials for drug delivery devices in ocular therapeutics. *ACS Appl. Mater. Interfaces* **2020**, *12*, 30189−30197.
(36) Ma, X.; Chai, Y.; Li, P.; Wang, B. Metal-organic framework films and their potential applications in environmental pollution control. *Acc. Chem. Res.* **2019**, *52*, 1461−1470.
(37) He, H.; Han, H.; Shi, H.; Tian, Y.; Sun, F.; Song, Y.; Li, Q.; Zhu, G. Construction of thermophilic lipase-embedded metal-organic frameworks via biomimetic mineralization: A biocatalyst for ester hydrolysis and kinetic resolution. *ACS Appl. Mater. Interfaces* **2016**, *8*, 24517−24524.
(38) Qi, L.; Luo, Z.; Lu, X. Biomimetic mineralization inducing lipase-MOF nanocomposite for pickering interfacial biocatalytic system. *ACS Sustain. Chem. Eng.* **2019**, *7*, 7127−7139.
(39) Lian, X.; Fang, Y.; Joseph, E.; Wang, Q.; Li, J.; Banerjee, S.; Lollar, C.; Wang, X.; Zhou, H.-C. Enzyme-MOF (metal-organic framework) composites. *Chem. Soc. Rev.* **2017**, *46*, 3386−3401.
(40) Bosch, M.; Yuan, S.; Rutledge, W.; Zhou, H.-C. Stepwise synthesis of metal-organic frameworks. *Acc. Chem. Res.* **2017**, *50*, 857−865.
(41) Van Vleet, M. J.; Vleet, V.; Weng, T. T.; Li, X. Y.; Schmidt, J. R. In situ, time-resolved, and mechanistic studies of metal-organic framework nucleation and growth. *Chem. Rev.* **2018**, *118*, 3681−3721.
(42) Nadar, S. S.; Rathod, V. K. Magnetic-metal organic framework (magnetic-MOF): A novel platform for enzyme immobilization and nanozyme applications. *Int. J. Biol. Macromol.* **2018**, *120*, 2293−2302.
(43) Wu, H.; Li, T.; Bao, Y.; Zhang, X.; Wang, C.; Wei, C.; Xu, Z.; Tong, W.; Chen, D.; Huang, X. MOF-enzyme hybrid nanosystem decorated 3D hollow fiber membranes for in-situ blood separation and biosensing array. *Biosens. Bioelectron.* **2021**, *190*, 113413.
(44) Chai, M.; Razavi Bazaz, S.; Daiyan, R.; Razmjou, A.; Ebrahimi Warkiani, M.; Amal, R.; Chen, V. Biocatalytic micromixer coated with enzyme-MOF thin film for CO_2 conversion to formic acid. *Chem. Eng. J.* **2021**, *426*, 130856.
(45) Wang, C.; Gao, J.; Cao, Y.; Tan, H. Colorimetric logic gate for alkaline phosphatase based on copper (II)-based metal-organic frameworks with peroxidase-like activity. *Anal. Chim. Acta* **2018**, *1004*, 74−81.
(46) Tan, H.; Li, Q.; Zhou, Z.; Ma, C.; Song, Y.; Xu, F.; Wang, L. A sensitive fluorescent assay for thiamine based on metal-organic frameworks with intrinsic peroxidase-like activity. *Anal. Chim. Acta* **2015**, *856*, 90−95.
(47) Qin, F.-X.; Jia, S.-Y.; Wang, F.-F.; Wu, S.-H.; Song, J.; Liu, Y. Hemin@metal-organic framework with peroxidase-like activity and its application to glucose detection. *Catal. Sci. Technol.* **2013**, *3*, 2761−2768.
(48) Cheng, X.; Zheng, Z.; Zhou, X.; Kuang, Q. Metal-organic framework as a compartmentalized integrated nanozyme reactor to enable high-performance cascade reactions for glucose detection. *ACS Sustain. Chem. Eng.* **2020**, *8*, 17783−17790.
(49) Zheng, H.-Q.; Liu, C.-Y.; Zeng, X.-Y.; Chen, J.; Lü, J.; Lin, R.-G.; Cao, R.; Lin, Z.-J.; Su, J.-W. MOF-808: A metal-organic framework with intrinsic peroxidase-like catalytic activity at neutral pH for colorimetric biosensing. *Inorg. Chem.* **2018**, *57*, 9096−9104.
(50) Liu, Y. L.; Zhao, X. J.; Yang, X. X.; Li, Y. F. A nanosized metal-organic framework of Fe-MIL-88NH_2 as a novel peroxidase mimic used for colorimetric detection of glucose. *Analyst* **2013**, *138*, 4526−4531.
(51) Xu, W.; Jiao, L.; Yan, H.; Wu, Y.; Chen, L.; Gu, W.; Du, D.; Lin, Y.; Zhu, C. Glucose oxidase-integrated metal-organic framework hybrids as biomimetic cascade nanozymes for ultrasensitive glucose biosensing. *ACS Appl. Mater. Interfaces* **2019**, *11*, 22096−22101.
(52) Zhong, X.; Xia, H.; Huang, W.; Li, Z.; Jiang, Y. Biomimetic metal-organic frameworks mediated hybrid multi-enzyme mimic for tandem catalysis. *Chem. Eng. J.* **2020**, *381*, 122758.
(53) Rao, B.; Zhou, R.; Dong, Q.; Liao, X.; Liu, F.; Chen, W.; Liu, X.; Min, Y.; Wang, Y. Efficient surface display of L-glutamate oxidase and L-amino acid oxidase on pichia pastoris using multi-copy expression strains. *Biotechnol. Bioprocess Eng.* **2020**, *25*, 571−579.
(54) Mentana, A.; Nardiello, D.; Palermo, C.; Centonze, D. Accurate glutamate monitoring in foodstuffs by a sensitive and interference-free glutamate oxidase based disposable amperometric biosensor. *Anal. Chim. Acta* **2020**, *1115*, 16−22.
(55) Pham, M.-H.; Vuong, G.-T.; Vu, A.-T.; Do, T.-O. Novel route to size-controlled Fe-MIL-88B-NH_2 metal-organic framework nanocrystals. *Langmuir* **2011**, *27*, 15261−15267.
(56) Arima, J.; Sasaki, C.; Sakaguchi, C.; Mizuno, H.; Tamura, T.; Kashima, A.; Kusakabe, H.; Sugio, S.; Inagaki, K. Structural characterization of L-glutamate oxidase from Streptomyces sp X-119-6. *Febs. J.* **2009**, *276*, 3894−3903.
(57) Liang, K.; Ricco, R.; Doherty, C. M.; Styles, M. J.; Bell, S.; Kirby, N.; Mudie, S.; Haylock, D.; Hill, A. J.; Doonan, C. J.; Falcaro, P. Biomimetic mineralization of metal-organic frameworks as protective coatings for biomacromolecules. *Nat. Commun.* **2015**, *6*, 7240.
(58) Kashefi, S.; Seyed, M. B.; Niyaz, M. M. Covalently immobilized laccase onto graphene oxide nanosheets: Preparation, characterization, and biodegradation of azo dyes in colored wastewater. *J. Mol. Liq.* **2019**, *276*, 153−162.
(59) Nagvenkar, A. P.; Gedanken, A. $Cu_{0.89}Zn_{0.11}O$, a new peroxidase-mimicking nanozyme with high sensitivity for glucose and antioxidant detection. *ACS Appl. Mater. Interfaces* **2016**, *8*, 22301−22308.

https://doi.org/10.1021/acs.jafc.2c01639
J. Agric. Food Chem. 2022, 70, 3785−3794